

# Excluded Volume in Protein Sidechain Packing

Edo Kussell, Jun Shimada, Eugene I. Shakhnovich\*

October 26, 2018

**Running title:** Sidechain Packing in Proteins

36 pages (including figure/table captions), 7 figures, 2 tables.

Department of Chemistry and Chemical Biology  
Harvard University  
12 Oxford Street  
Cambridge MA 02138

\*corresponding author  
tel: 617-495-4130  
fax: 617-496-5948  
email: eugene@belok.harvard.edu

## Abstract

The excluded volume occupied by protein sidechains and the requirement of high packing density in the protein interior should severely limit the number of sidechain conformations compatible with a given native backbone. To examine the relationship between sidechain geometry and sidechain packing, we use an all-atom Monte Carlo simulation to sample the large space of sidechain conformations. We study three models of excluded volume and use umbrella sampling to effectively explore the entire space. We find that while excluded volume constraints reduce the size of conformational space by many orders of magnitude, the number of allowed conformations is still large. An average repacked conformation has 20% of its  $\chi$  angles in a non-native state, a marked reduction from the expected 67% in the absence of excluded volume. Interestingly, well-packed conformations with up to 50% non-native  $\chi$ 's exist. The repacked conformations have native packing density as measured by a standard Voronoi procedure. Entropy is distributed non-uniformly over positions, and we partially explain the observed distribution using rotamer probabilities derived from the pdb database.<sup>1</sup> In several cases, native rotamers which occur infrequently in the pdb database are seen with high probability in our simulation, indicating that sequence-specific excluded volume interactions can stabilize rotamers that are rare for a given backbone. In spite of our finding that 65% of the native rotamers and 85% of  $\chi_1$  angles can be correctly predicted on the basis of excluded volume only, 95% of positions can accommodate more than 1 rotamer in simulation. We estimate that in order to quench the sidechain entropy observed in the presence of excluded volume interactions, other interactions (hydrophobic, polar, electrostatic) must provide an additional stabilization of at least 0.6 kT per residue in order to single out the native state.

**Keywords:** sidechain packing, packing density, protein folding, protein structure prediction

# Introduction

One remarkable characteristic of proteins is that sidechains comprising the hydrophobic core are as closely packed as organic crystals.<sup>2</sup> In most proteins with known 3D structures, the core residues are rarely disordered and adopt one of a small number of alternative conformations. This almost unique packing is effected by a combination of steric interactions (excluded volume effects) and energetic stabilization (hydrophobic, polar, and charge interactions). The proportions by which these interactions contribute to the overall stability is unknown, but several studies suggest that steric and hydrophobic interactions are of primary importance.<sup>3,4</sup>

Sidechain packing has been studied intensively for various reasons, notably: 1) It is thought to be a crucial piece of the protein folding puzzle;<sup>5,6</sup> 2) The selection of protein sequences through evolution may have been influenced by how well a sequence can be packed for a particular fold;<sup>4</sup> 3) Accurate packing algorithms are necessary for complete protein structure prediction; and 4) Existing threading and homology modeling algorithms may be significantly improved by a better understanding of how sidechains are stabilized in the core.<sup>7,8</sup> A plethora of computational methods for modeling protein sidechains and energetics exist,<sup>3,7,9,10</sup> and yet which ones best capture the underlying physics is unclear. This is due, in part, to the use of energy functions containing many different types of interactions.

In this paper, we examine the role of excluded volume in isolation of all other types of interactions. This allows us to address the importance of geometry in determining the native state of protein sidechains. We use an all-atom, rotamer-based model of a protein to obtain repacked conformations of its interior sidechains. By choosing the most realistic representation of sidechain and backbone geometries, we eliminate errors encountered in coarse-grained models.

Because there is no consensus on how excluded volume interactions should be modeled in the context of proteins, we consider three different models. The simplest model treats all heavy atoms as hard spheres which are not allowed to overlap. The second model further restricts the sterically allowed space by adding a second shell around the hard spheres which tolerates only a limited number of overlaps throughout the entire protein. The third model uses a continuous  $r^{-12}$  potential, which is the repulsive contribution from a Lennard-Jones potential. Since a potential which decays faster than our chosen  $r^{-12}$  potential would allow more sidechain conformations, and since a slower decaying function is generally not used to model sterics,<sup>11</sup> the three we have chosen should cover most of the possibilities as far as models featuring spherically symmetric, atom-based potentials.

For each model, we obtain the distribution of rms values for sidechain conformations satisfying excluded volume constraints. This amounts to a full characterization of the ground-state ensemble of protein sidechains subject to excluded volume effects only. We find a vast number of significantly different conformations with native-like packing density that meet excluded volume constraints, implying that excluded volume alone cannot stabilize the native conformation of sidechains even when the backbone is fixed. We provide an estimate for the amount of additional stabilization that must be provided through interactions other than sterics. The results obtained using three different models are consistent with each other, suggesting that our main conclusions are model-independent. We also examine the correlation between our simulations and the distribution of rotamers in the pdb database, and discuss implications for sidechain prediction. Our main goal is to elucidate the role of excluded volume in establishing the ensemble of conformations compatible with the folded state of a protein.

## Methods

**All-Atom Protein Representation.** Three proteins were used in this study: photoactive yellow protein (1F9I), subtilisin (1GCI), and concanavalin (1NLS). We chose these proteins because they have very high resolution crystal structures, and are of different secondary-structure classes: subtilisin is a 0.78 Å resolution structure, and is an all  $\alpha$ -helical protein; concanavalin (0.94 Å resolution) is all  $\beta$ -sheet; and photoactive yellow protein (1.1 Å resolution) is  $\alpha/\beta$ . All heavy atoms of the proteins present in the crystal structure were represented. Each sidechain torsion was allowed to take on one of three rotamer values<sup>1</sup> plus a random noise of  $\pm 10^\circ$ . Rotamer probabilities<sup>1</sup> were not used in the simulation. At all times, the atoms of the entire backbone were kept fixed in their original crystal structure positions.

**Models of sterics.** The excluded volume interactions of protein sidechains were modeled in three ways:

- 1) In the *hard-sphere model* atoms were treated as impenetrable spheres of given radii. These hard-sphere radii are necessarily smaller than the van der Waals (vdW) radii, and were defined by scaling the vdW radii by some factor  $\alpha_h$ . All atom-atom interactions at distances smaller than the sum of the hard-sphere radii (“hard clashes”) were strictly forbidden. A pair of atoms  $i$  and  $j$  separated by a distance  $r_{ij}$  is said to be a hard clash if  $r_{ij} < \alpha_h (r_0(i) + r_0(j))$ , where  $r_0(i)$  is the vdW radius of atom  $i$ . The set of vdW radii determined in<sup>12</sup> was used.  $\alpha_h$  was taken to be the largest value such that all hard clashes in the native protein conformation can be eliminated within the  $\pm 10^\circ$  allowed at each torsion; we found that  $\alpha_h = 0.76$  for concanavalin and photoactive yellow protein, and 0.77 for subtilisin. The steric energy,  $U_h$ , of a conformation in this model is given by the number of hard clashes. Only conformations with  $U_h = 0$  are sterically allowed in this model.

2) Since results could depend on the choice of  $\alpha_h$ , we explored a *soft-sphere model* in which atoms consisted of two radii - the hard-sphere radii fixed by  $\alpha_h$ , and somewhat larger, soft-sphere radii. Soft radii were defined by scaling vdW radii by a parameter  $\alpha_s$ , where  $\alpha_h < \alpha_s \leq 1$ . A soft clash occurs when  $\alpha_h (r_0(i) + r_0(j)) < r_{ij} < \alpha_s (r_0(i) + r_0(j))$ . All hard clashes were forbidden as before, while only a limited number of soft clashes are allowed over the entire protein. The steric energy,  $U$ , of a conformation is given by  $U = U_h + U_s$ , where  $U_h$  is the number of hard atom-atom clashes, and  $U_s$  is the number of soft atom-atom clashes above threshold. The threshold number of soft clashes allowed is a function of  $\alpha_s$ , as described in Fig. 1. Only conformations with  $U = 0$  are sterically allowed in this model. Since van der Waals radii are strictly greater than excluded volume radii, as demonstrated in numerous studies of gas phase organic molecules,<sup>11</sup>  $\alpha_s$  must be strictly less than 1.0, and we include  $\alpha_s = 1.0$  in our plots only as an upper limit on the radii.

3) The third model used the repulsive term of a *Lennard-Jones* potential. For each pair of atoms we fit the LJ potential,  $A/r^{12} - 1/r^6$ , so that the minimum coincides with the sum of the vdW radii taken from.<sup>12</sup> With this model, the steric energy of a conformation is given by  $U_{LJ} = \sum_{ij} A_{ij}/r_{ij}^{12}$  where the sum is taken over all pairs of atoms, and  $A_{ij} = (r_0(i) + r_0(j))^6/2$ . We considered a conformation to be sterically allowed if its energy was less than or equal to the energy of the native crystal structure.

**Monte Carlo Packing Algorithm.** Initial random sidechain conformations were packed to a given rms interval  $[R_{min}, R_{max}]$  by a Metropolis Monte Carlo simulation.<sup>13,14</sup> At each step of the simulation, a random position was selected and changed to another rotamer. The move was

accepted with probability  $p$  given by

$$p = \begin{cases} 1 & \delta H \leq 0 \\ \exp(-\delta H/T) & \text{otherwise} \end{cases}$$

with

$$\delta H = \delta U + \begin{cases} C(R_{min} - R) & R < R_{min} \\ 0 & R_{min} \leq R \leq R_{max} \\ C(R - R_{max}) & R > R_{max} \end{cases}$$

where  $U$  is the steric energy,  $R$  is the rms, and  $C = 10$ . All reported rms values were computed over the subset of sidechains having more than 40% occluded surface area as defined in reference 15, and at least 1 rotatable  $\chi$  angle. All heavy atoms of a sidechain, including the  $C_\beta$  atom, entered into the rms calculation as in reference 3. Prolines were kept fixed in their crystal structure positions throughout this work. The 40% occluded positions for each protein are given below. Additionally, by visual inspection we found positions whose  $C_\alpha$ - $C_\beta$  bonds were pointing toward the core, and/or whose sidechains were surrounded by other atoms on all sides. These positions are indicated in bold type.

Subtilisin:

(1) **8I,11V**,17H,21L,22T,**26V**,27K,**28V**,**30V**

(10) **31L,32D,33T,35I**,36S,38H,40D,**41L**,49F,50V

(20) **58D**,62H,**64T,65H,66V,69T,70I**,73L,79V,80L

(30) **82V**,87E,**88L**,89Y,**91V,92K,93V**,94L,**104S**,105I

(40) **109L**,111W,117M,**119V,121N,122L**,123S,130S,133L,137V



(50) 139S,141T,145V,146L,**147V**,**148V**,**151S**,**159I**,160S,161Y  
(60) 165Y,**169M**,**171V**,**174T**,175D,183F,**184S**,185Q,186Y,**190L**  
(70) 191D,**192I**,**193V**,197V,199V,**201S**,**202T**,203Y,**214T**,215S  
(80) 216M,**218T**,**220H**,**221V**,**227L**,**228V**,229K,232N,237N,240I  
(90) 241R,243H,**244L**,245K,256L,257Y,261L,**262V**,263N,265E  
(100)268T

Concanavalin:

(1) 4I,5V,**7V**,**8E**,**9L**,**10D**,11T,14N,17I  
(10) **19D**,**24H**,**25I**,**27I**,**28D**,29I,31S,**32V**,**40W**,**52I**  
(20) **54Y**,55N,**61L**,62S,**65V**,67Y,75V,79V,80D,**81L**  
(30) **85L**,**89V**,90R,**91V**,**93L**,**94S**,**96S**,**97T**,**102E**,103T  
(40) **104N**,**105T**,**106I**,108S,**109W**,**110S**,**111F**,113S,115L,117S  
(50) **128F**,130F,**133F**,**134S**,**140L**,143Q,145D,148T,153N,154L  
(60) **156L**,**157T**,164S,169S,170V,**172R**,174L,175F,179V,**180H**  
(70) **191F**,195F,196T,**197F**,**199I**,**201S**,208D,**210I**,211A,**213F**  
(80) **214I**,215S,216N,**219S**,**225S**,229L,**230L**,**232L**,233F

Photoactive Yellow Protein:

(1) 6F,**11I**,12E,**15L**,18M,22Q,23L,**26L**,28F  
(10) **31I**,32Q,**33L**,34D,38N,**39I**,41Q,**42F**,43N,**46E**  
(20) 49I,**50T**,57V,61N,62F,**63F**,**66V**,**70T**,72S,**75F**  
(30) 76Y,79F,83V,88L,90T,92F,**96F**,**105V**,106K,**107V**

(40) 108H,109M,**110K**,111K,**117S**,**118Y**,119W,**120V**,**121F**,122V

**Umbrella sampling.** Umbrella sampling<sup>16</sup> was used to determine the number of states  $\Omega(R)$  for each of the 3 models. First, different sterically allowed conformations were collected for rms intervals of size  $0.05 \text{ \AA}$  over the entire rms range ( $0 - 4.0 \text{ \AA}$ ). The rms values of conformations differing only by random noise were averaged. Next, the probability to observe a conformation with rms  $R$ ,  $p_i(R)$ , was obtained for the  $i$ -th rms interval,  $[R_i, R_{i+1}]$ . Since the distribution of conformations  $\Omega(R)$  must be a continuous function of  $R$ ,  $\Omega(R)$  can be determined by appropriately scaling the probabilities  $p_i(R)$  to ensure continuity at interval boundaries. Specifically, the probabilities  $p_i(R)$  are sequentially scaled by  $p_{i-1}(R_i)/p_i(R_i)$ , starting from  $i = 2$ .  $\Omega(R)$  is then obtained by multiplying all rescaled  $p_i$ 's by  $\Omega(R_1)/p_1(R_1)$ .

The umbrella sampling scheme can only work provided that the conformational space within each bin is explored evenly during simulation. In order to move the system into a particular rms bin, we had to use  $C = 10$  and work at very low temperature ( $T = 0.005$ ). These conditions were necessary due to the large amount of entropy available just outside any given bin, both in rms and in steric energy (the number of clashed conformations is exponentially larger than the number of well-packed ones). The downside is that the system may end up in a part of conformational space within a given bin that is disconnected from other parts of the bin, i.e. the system behaves non-ergodically under the conditions in which it must be sampled. The rms histograms within such isolated clusters are not representative of the entire space within a bin, and can therefore lead to large errors when the full rms histogram is assembled. To overcome this difficulty, we performed 200 short runs, starting from random conformations, for each bin and computed the size of the cluster explored in each run. The cluster size is defined as the average torsional distance between all pairs

of uncorrelated conformations encountered in a run. We found that most bins had many clusters of various sizes. Since the number of states within a cluster should scale exponentially with its size, the largest cluster encountered should dominate the statistics within a given bin. We therefore sampled each bin by starting a run from a conformation obtained in a short run that had entered the large cluster. For every rms bin, we collected 10,000 states in the largest cluster, and used only these states when assembling the full rms histogram.

Several tricks proved handy when trying to find the large cluster. The plot of the largest cluster's size over rms should be relatively smooth. If we found a cluster of size 20 at rms 0.90, a cluster of size 10 at rms 0.95, and a cluster of size 24 at rms 1.00, we could be certain that the 0.95 bin would be badly sampled. We could thus focus our efforts on bins with anomalously low cluster sizes. Some bins required up to 500 short runs before the large cluster was found. We observed that there is only one cluster at low rms values. If we started a run from the lowest rms bin, and allowed it to escape into a higher rms bin, the run would always end up in the largest cluster for that bin. This worked up to rms 1.2 because entropy was steeply increasing with rms, and one cluster was dominating the statistics. For rms values between 1.2 and 2.0, several clusters of similar sizes emerged, and thus sampling the largest one was no longer adequate. In this rms range, the distribution of states was relatively flat over rms, and thus the entire range could be fully sampled as a single large bin. For rms higher than two, the method of multiple short runs worked well. The distribution of clusters as rms is varied emerged as an interesting problem in itself, but was beyond the scope of this paper.

**CHARMM minimization of structures** Using CHARMM, we minimized and added hydrogen atoms to a set of 50 randomly chosen repacked conformations of each of the three proteins used in this study. All such minimizations, including those performed for other randomly selected packed

structures, did not change the rotamer states of the sidechains, but did eliminate close contacts (as defined by CHARMM) resulting from the addition of hydrogens. A set of 1000 repacked conformations are available for public download at <http://www-shakh.harvard.edu/~shimada/index.html>.

## Results

Figure 2 shows the distribution of *packed* (sterically allowed) conformations for three proteins, obtained over a range of rms values using umbrella sampling. For each protein, the rms values are computed over the subset of partially occluded residues (see Methods), and thus only the occluded positions contribute to the total number of states. All other positions are free to repack, but are not counted in our sampling. With  $\alpha_s = \alpha_h$  (the hard-sphere model), the number of packed conformations of subtilisin is approximately  $10^{32}$ . As  $\alpha_s$  is increased using the soft-sphere model, the number of packed conformations decreases. This trend reverses when the soft radii reach the van der Waals size (see Discussion), at  $\alpha_s = 1.0$ , and the number of repackings is approximately  $10^{19}$ . We emphasize that the soft-sphere model tolerates fewer clashes than the hard-sphere model, because it allows no hard-sphere clashes (at  $\alpha_h$ ) and only a limited number of soft-sphere clashes (at  $\alpha_s$ ). Using the steric LJ model, the number of repackings is  $10^{25}$ . Since the number of repackings scales exponentially in the number of free torsions, we give the number of rotamer states per torsion in Table 2 for each protein, calculated from the LJ model. These numbers are obtained by taking the  $n$ -th root of the total number of states, where  $n$  is either the number of free torsions or residues. Normalizing by the number of torsions gives smaller variation over proteins than when normalizing by number of residues, due to compositional differences between proteins (variation in number of torsions per residue among proteins).

As a control, we applied the same sampling method to obtain the distribution of states for all possible sidechain conformations, packed and not packed, as shown in Figure 3. The total number of random sidechain conformations for a protein with  $n$  free torsions is  $3^n$ . For all three proteins, the area under the random curve obtained from umbrella sampling is  $n \log(3) \pm 2$ , demonstrating that the sampling is reliable, and that the total error is approximately 2 orders of magnitude. For each protein we included the distribution of states using the hard-sphere model (dashed line) in order to show the dramatic reduction in available conformations once excluded volume constraints are applied.

In Figure 4 we show the sampling of packed conformations for subtilisin without umbrella constraints. The same data is shown separately over rms and over torsional distance from the native conformation. We see that the distributions over rms for the different steric models often yield two humps. When plotted over torsional distance, all models give perfect normal distributions. We found no correlation between rms and torsional distance in the range of rms that was sampled without umbrella constraints. One reason for this lack of correlation is that deviations in the  $\chi_1$  angle yield much larger deviations in rms than the other  $\chi$  angles. Thus, unless rms is very low, it yields almost no information about the torsional states of the protein.

The packing density of a conformation is usually defined as the volume of the van der Waals envelope of a protein divided by its Voronoi volume. The density of a random sample of 1000 repacked conformations of each protein was computed and found to vary by only  $\pm 1\%$  of the native density. Given this minimal variation in packing density, we conclude that the requirement of having native-like density does not significantly reduce the number of packed sidechain conformations. In addition, we were able to build hydrogen atoms (using CHARMM<sup>17</sup>) on randomly selected, packed conformations, confirming that the conformations were not too compact.

While the number of packed conformations is large, it is conceivable that most repackings are structurally similar to one another, and thus that the number of truly different repackings may be much smaller than observed. To determine how different these repacked conformations are, we uniquely identified each conformation by the rotamers of the partially occluded positions. The distance between two conformations was measured by counting the number of single-bond torsions which had to be rotated (by  $120^\circ$ ) in order to obtain one conformation from the other. For example, for the partially occluded positions of subtilisin, having a total of 174 torsions, we expect random conformations to differ by 115 ( $= 174 \times 2/3$ ) torsion moves.

The average torsional distance between repacked conformations (Fig. 2) shows that the conformations are different from each other. The similarity between conformations depends on the particular model. In general, larger soft radii lead to more similar repackings until the soft radii reach the van der Waals size (see Discussion). For the three proteins we examined, average conformations obtained with the LJ model differ at 20%-25% of their torsions. We note that the differences between the soft-sphere models for  $\alpha_s \geq 0.90$  and the LJ model are minimal in all three proteins.

The entropy of each sidechain was computed by sampling uncorrelated states meeting the LJ constraints for each protein (Fig. 5). The plot shows that entropy is not distributed evenly over positions. Approximately 25% of positions have nearly zero entropy, implying that they are rarely repacked. We note that only 5% of positions have exactly zero entropy, demonstrating that almost all positions can accommodate more than one rotamer. The maximum entropy possible for a sidechain with  $n$  torsions is  $n \ln(3) = 1.1n$ . Since we observe positions with entropy greater than 1.1, it is clear that large residues can take on several different rotamers.

To explain the uneven distribution of entropy, we tried to correlate it with various quantities.

The entropy of a given position showed no correlation with either crystallographic B-factors, or with occluded surface area. We found significant but relatively low correlation ( $R = 0.65$ ) between the entropies we observed and entropies calculated from rotamer probabilities from the PDB database.<sup>1</sup> To investigate this trend further, we plotted the rotamer probabilities observed in our simulation versus probabilities observed in the pdb database. Specifically, for each rotamer state at every partially occluded position we plotted the frequency with which it was observed in our simulation, versus the frequency with which it occurs in the pdb database at its particular  $\phi$  and  $\psi$  backbone angles.

These scatter plots for the three proteins are shown in Figure 6. The plots indicate that native rotamers (red marks, corresponding to the rotamers observed in the crystal structure) are often seen with high probability in our simulations. Since we observe in simulations only a few non-native rotamers (blue marks) with probability greater than 90%, the low entropy positions in Figure 5 largely correspond to the native conformation. The pdb probabilities are obtained by averaging over many different folds and sequences, and thus sequence-specific effects are largely averaged out, leaving only the backbone  $\phi$  and  $\psi$  angles as a determinant of rotamer frequency. Hence the simulation frequency of rotamers lying near the diagonal is explained well by the local backbone conformation at that position. Rotamers lying off the diagonal are being observed with anomalous frequency for their local backbone conformation. Because the backbone conformation does not explain the frequency of these positions, they must be particularly sensitive to one or more sequence-specific interactions. We observe several native rotamers with anomalously high probability (upper-left corner), indicating that sequence-specific steric interactions can completely stabilize the native rotamer even when it is rarely observed in most other proteins. We see a few non-native rotamers anomalously frequently (blue marks in the upper-left of the figure). These

rotamers are preferentially selected by sequence-dependent excluded volume interactions over the native rotamers.

One can classify positions, loosely speaking, as either “well-predicted” if the correct native rotamer is seen more than 50% of the time, or “poorly-predicted” if the native rotamer is seen less than 50% of the time. Non-native rotamers are plotted as squares if they belong to “well-predicted” positions, and circles if they belong to “poorly-predicted” positions. A non-native rotamer which is seen with high probability in the PDB database, may be seen with low probability in our simulation, lying in the bottom-right corner of the figures. Most points in this region are squares, that is, non-native rotamers which are being seen too infrequently because they belong to “well-predicted” positions. There are very few circles in this region indicating that, for the most part, significant deviations from observed pdb rotamer probabilities are due to sequence-specific interactions stabilizing the native rotamer preferentially over a more popular rotamer.

Concanavalin appears to have more scatter than the other two proteins. In particular, it has more native rotamers below and near the diagonal. Concanavalin is an all- $\beta$  protein, while subtilisin is all- $\alpha$ , and photoactive yellow protein is  $\alpha/\beta$ . It is likely that the  $\alpha$ -helices of subtilisin, which act to compactify the fold locally, impose more stringent constraints on the allowed rotamers at a given position. This is manifested in our observation of fewer near-diagonal native rotamers in subtilisin than in concanavalin.

To check whether simulation probabilities correlate with amino acid type, we plotted the sequence identity of the native rotamers as letters in Figure 7. We see that points lying in the lower left-hand corner are generally polar or charged amino acids. Native rotamers seen with high probability in simulation are mostly hydrophobic. There are exceptions to both of these general trends. Since hydrophobic residues are on average more buried than charged residues, one might



suggest that the separation based on polarity is actually due to solvent-exposure. As stated above, however, we found no correlation between occluded surface and the simulation probabilities. In order to verify that this was not due to some peculiarity of the definition of occluded surface, we visually classified positions as buried or partially exposed using rough criteria outlined in Methods. The purple letters in Figure 7 correspond to buried positions (as defined in Methods), while the green letters correspond to partially exposed positions. We see no significant clustering of either color in these figures, confirming that entropy in our simulations is not governed by exposure. We conclude, not surprisingly, that the importance of electrostatic interactions, rather than solvent exposure, explains the poorly-predicted native rotamers of charged amino acids.

We examined the correlation between the rotamer changes made at a pair of positions  $x$  and  $y$  by measuring the number of states lost,  $\exp(\Delta S)$ , due to interactions between  $x$  and  $y$ , where  $\Delta S = S_{xy} - (S_x + S_y)$ ,  $S_{xy}$  is the joint entropy, and  $S_x$  and  $S_y$  are the individual entropies. We found only 3 pairs of positions in subtilisin exhibiting any correlation ( $\exp(\Delta S)$  between 0.1 and 0.3). Similar numbers were found in the other two proteins. Repacking at a single position can therefore be accommodated by the surrounding residues in many different ways.

Given that there is a significant amount of torsional entropy in our model, it is interesting to ask how well an average sidechain structure prediction based solely on excluded volume would perform. For subtilisin, we observe the rms of predictions broadly distributed between 1.4 and 1.8 angstroms. Using either the LJ model or the  $\alpha_s = 0.90$  model, we predict correct rotamers for 65% of residues, and predict  $\chi_1$  angles correctly for 85% of positions. The best performing sidechain prediction algorithms, which incorporate several physical and knowledge-based terms, predict 93% of  $\chi_1$  angles, so excluded volume alone performs very well in this regard.

## Discussion

Upon folding to its native backbone topology, the conformational space of a protein is cut by many orders of magnitude (Fig. 3) due to excluded volume. At the level of a single torsion, the number of rotamer states is reduced by approximately a factor two. The native backbone can still accommodate many different sidechain conformations, while maintaining its high degree of compactness. Other sources of stabilization (such as attractive van der Waals interactions, hydrogen bonding, polar interactions) are necessary to overcome the final entropic cost associated with fixing the sidechains in their native conformations.

The packing of sidechains in a native backbone has often been described as a jigsaw-puzzle: the shapes of the sidechains (the pieces) are enough to determine how they will fit in the protein interior.<sup>18</sup> This argument has been used to explain the high density observed in proteins. The large number of repackings and the diversity of these conformations (Fig. 2), all with native-like density, suggest that a precise fitting of residues is not necessary for a high packing density. The rotamer frequency plots demonstrate that while there is a sequence-specific excluded volume effect that acts to single out the native rotamers, it is not sufficient to overcome the fact that the backbone generally allows several different rotamers at each position. The distribution of entropy shows that many positions admit significantly more than one rotamer. Furthermore, the correlation calculations show that a conformational change at one position does not necessitate a particular change at spatially proximate positions. We conclude that while sidechains must fit together to avoid steric clashes and maintain native-like density, these constraints alone do not give rise to precise and unique fitting of residues. Other energetic interactions must bias sidechain conformations toward the native state, leading to the observation of directional packing in protein structures.<sup>19</sup>

The three models employed in our study yield consistent results. All three vastly reduce the total number of available states. The hard-sphere model is consistently more forgiving than the other models. The soft-sphere models with  $\alpha_s \geq 0.90$  all roughly agree to  $\pm 2$  orders of magnitude. The LJ model is only slightly more tolerant than the soft-sphere models, suggesting that a two-shell model can adequately model sterics without introducing continuous distance dependence. The soft-sphere model has two limiting behaviors. For  $\alpha_s = \alpha_h$ , the soft-sphere model is identical to the hard-sphere model. For  $\alpha_s \gg 1$ , all atom pairs in the *native* structure are considered to clash, and thus the soft-sphere model will tolerate all possible clashes. Since the hard-sphere excluded volume is the only remaining constraint, the soft-sphere model is again equivalent to the hard-sphere model in this limit. The observed rise in the number of states as  $\alpha_s$  reaches 1.0 is the necessary turn-around between these two limiting behaviors. Sterics must therefore be modelled with  $\alpha_s < 1$ . When  $\alpha_s = 1.0$ , the radii have reached van der Waals sizes, and are in the regime of attraction rather than excluded volume. While increasing the radii past the hard-core value gives a significant gain in stability, we see that there is a limit on how much stabilization can be achieved from excluded volume effects.

Our ability to predict 85% of  $\chi_1$  angles correctly shows that excluded volume is of primary importance in determining the general orientation of a sidechain with respect to its backbone. Our prediction of only 65% of positions correctly shows that sterics are less important in determining the rest of the sidechain's rotameric conformation. Of particular interest are native rotamers that are observed in the PDB database in less than 10% of proteins. Many of these rotamers are observed with significantly higher probability in our simulation, while some are observed at their expected PDB level. The excluded volume interaction is thus exhibiting some frustration between the distribution of states compatible with the local backbone conformation, and the sequence-

specific neighborhood of the residue. Other interactions must provide significant stabilization to overcome this problem.

A natural extension of our work is to add an attractive interaction to the potential which would stabilize the native packing. From the distribution of packed conformations, we estimate that the native conformation must be about  $0.6kT$  per sidechain (see Table 2) lower in energy than the average packed conformation with native backbone. This estimate can be used to guide efforts towards designing better potentials for sidechain packing. Furthermore, the techniques presented here, combined with a stepwise increase in the complexity of potentials, can determine how much stabilization each additional interaction provides. It will be interesting to see whether a potential that significantly stabilizes the native rotamers can stabilize the native fold when backbone motions are added to the model.

## Acknowledgements

We are grateful for stimulating discussions with Gabriel Berriz, Alexey Finkelstein, Leonid Mirny, and Michael Morrissey, and especially thank Kirk Doran for his assistance. Financial support from NIH (grant 52126) and NSF (graduate fellowship, E.K.) is acknowledged.

## References

1. Dunbrack, Jr., R. L. & Cohen, F. E. (1997). Bayesian statistical analysis of protein side-chain rotamer preferences. *Protein Sci.* **6**, 1661–1681.
2. Fersht, A. (1999). *Structure and Mechanism in Protein Science*. W. H. Freeman and Company, New York, 1st ed.
3. Lee, C. & Subbiah, S. (1991). Prediction of protein side-chain conformation by packing optimization. *J. Mol. Biol.* **217**, 373–388.
4. Ponder, J. W. & Richards, F. M. (1987). Tertiary templates for proteins. *J. Mol. Biol.* **193**, 775–791.
5. Richards, F. M. & Lim, W. A. (1994). An analysis of packing in the protein folding problem. *Quat. Rev. Biophys.* **26**, 423–498.
6. Shakhnovich, E. I. & Finkelstein, A. V. (1989). Theory of cooperative transitions in protein molecules. i. why denaturation of globular proteins is a first-order phase transition. *Biopolymers* **28**, 1667–1680.
7. Bower, M. J., Cohen, F. E. & Dunbrack, R. L. (1997). Prediction of protein side-chain rotamers from a backbone-dependent rotamer library: A new homology modeling tool. *J. Mol. Biol.* **257**, 1268–1282.
8. Mirny, L. A. & Shakhnovich, E. I. (1998). Protein structure prediction by threading. why it works and why it does not. *J. Mol. Biol.* **283**, 507–526.

9. Petrella, R. J., Lazaridis, T. & Karplus, M. (1998). Protein sidechain conformer prediction: a test of the energy function. *Folding & Design* **3**, 353–377.
10. Mendes, J., Baptista, A. M., Carrondo, M. A. & Soares, C. M. (1999). Improved modeling of side-chains in proteins with rotamer-based methods: A flexible rotamer model. *Proteins* **37**, 530–543.
11. McQuarrie, D. A. (1976). *Statistical Mechanics*. Harper Collins, New York, 1st ed.
12. Tsai, J., Taylor, R., Chothia, C. & Gerstein, M. (1999). The packing density in proteins: Standard radii and volumes. *J. Mol. Biol.* **290**, 253–266.
13. Metropolis, N., Rosenbluth, A. W., Rosenbluth, M. N., Teller, A. H. & Teller, E. (1953). Equation of state calculations by fast computing machines. *J. Chem. Phys.* **21**, 1087–1092.
14. Binder, K. & Heerman, D. W. (1992). *Monte Carlo Simulation in Statistical Physics*. Springer-Verlag, Berlin, 2nd ed.
15. Pattabiraman, N., Ward, K. & Fleming, P. (1995). Occluded molecular surface: Analysis of protein packing. *Journal of Molecular Recognition* **8**, 334–344.
16. Chandler, D. (1987). *Introduction to Modern Statistical Mechanics*. Oxford, New York, 1st ed.
17. Brooks, B. R., Bruccoleri, R. E., Olafson, B. D., States, D. J., Swaminathan, S. & Karplus, M. (1983). CHARMM: a program for macromolecular energy, minimizations and dynamics calculations. *J. Comput. Chem.* **4**, 187.

18. Levitt, M., Gerstein, M., Huang, E., Subbiah, S. & Tsai, J. (1997). Protein folding: The endgame. *Annu. Rev. Biochem.* **66**, 549–79.
19. Mitchell, J. B. O., Laskowski, R. A. & Thornton, J. M. (1997). Non-randomness in side-chain packing: The distribution of interplanar angles. *Proteins* **29**, 370–380.



# Figures

## Figure 1

The number of soft clashes in near-native conformations as a function of  $\alpha_s$  for each protein studied. The solid line denotes the average number observed in an ensemble of near-native conformations generated by adding  $\pm 10^\circ$  random noise to the native sidechains. The dotted line is determined by taking three standard deviations below the average, and corresponds to the soft clash threshold used in this study.

## Figure 2

The figures in the left column show the density of packed conformations as a function of rms for various values of  $\alpha_s$  (indicated by the colored, solid curves). The dashed curve is the corresponding distribution using the repulsive Lennard-Jones model. Figures in the right column show the average number of bond rotations needed to bring one conformation to another as a function of rms for the various models. The average is taken over all pairs of 1000 randomly selected conformations found in a given rms window.

## Figure 3

The distribution of random sidechain conformations for each of the three proteins (solid lines). Umbrella sampling over rms without any excluded volume constraints was used to construct these figures. The dashed lines correspond to the hard-sphere model (identical to the black curves from Figure 2) and are provided for comparison.

#### Figure 4

Uncorrelated packed conformations for subtilisin sampled using the various models with no rms constraints are histogrammed separately over rms from the native crystal structure, and over torsional distance from the native rotamers. Each histogram is obtained over a total of 240,000 states. The states shown in this plot correspond to the tops of the rms histograms from Figure 2, but were obtained without umbrella sampling. We therefore do not see any low rms states in these plots, because there are exponentially fewer states as rms is lowered. The native rotamer configuration of subtilisin was obtained by minimizing rms in simulation. The rms of this nearly-native rotameric state is 0.5 Å from the crystal structure. The reason for the non-zero rms is that deviations of more than 10 degrees from perfect rotamers are observed in the crystal structure, and our simulations allows for no more than 10 degrees of tolerance around each rotameric value for a given sidechain  $\chi$  angle.

#### Figure 5

The entropy for the partially occluded positions of each protein. 50,000 uncorrelated packed conformations were sampled for each protein using the repulsive LJ model without umbrella sampling. The probability of observing each rotamer at each position was calculated, and the entropy of each position was computed using  $S = -\sum p_i \log p_i$ , where  $p_i$  is the frequency of occurrence of the  $i$ -th rotamer at the given position. The histograms of these entropy values are also provided for each protein.

#### Figure 6

Observed simulation frequency of a rotamer vs. the PDB database frequency of that rotamer,

given its amino acid identity and the  $\phi$ - $\psi$  angles of its backbone. Database probabilities were taken from the rotamer library described in.<sup>1</sup> Each point in the plots corresponds to a single rotamer. Red points are native rotamers (there is one red point for each sequence position); blue points are non-native rotamers (there are multiple blue points for each position). We called positions “well-predicted” if the native rotamer was observed more than 50% of the time, and “poorly-predicted” otherwise. We further classified the non-native rotamers (blue points) as squares if they belonged to “well-predicted” positions or circles if they belong to “poorly-predicted” positions. For example, if a native rotamer at a given position is observed 85% of the time, all the other, non-native rotamers for that position will be squares. Conversely, if at a different position the native rotamer is seen only 15% of the time, all the non-native rotamers for that position will be circles. Simulation frequencies are calculated over 50,000 packed conformations obtained using the LJ model without umbrella sampling.

### Figure 7

Simulation vs. PDB frequency for each *native* rotamer. The native rotamers for each protein are identified by their amino acid type (letter) and are colored purple if they are in a buried position, and green if they are in a partially exposed position. The buried positions are given in the methods section, indicated in bold type.

## Tables

atomic group	$r$	$\alpha_h r$
C3H0	1.61	1.21
C3H1	1.76	1.32
C4H1	1.88	1.41
C4H2	1.88	1.41
C4H3	1.88	1.41
N3H0	1.64	1.23
N3H1	1.64	1.23
N3H2	1.64	1.23
N4H3	1.64	1.23
O1H0	1.42	1.07
O2H1	1.46	1.10
S2H0	1.77	1.33
S2H1	1.77	1.33

Table 1:

### Table 1

The atomic groups, VdW radii ( $r$ ), and the hard core distances ( $\alpha_h r$ ) used in our study. The atom groups and VdW radii were obtained from Table 2 of Tsai *et al.* (1999). The atomic group  $AnHm$  refers to an atom of element A with a chemical valence of  $n$  and  $m$  hydrogen atoms bonded to it. A methyl carbon ( $-\text{CH}_3$ ), for example, falls under the C4H3 atomic group.

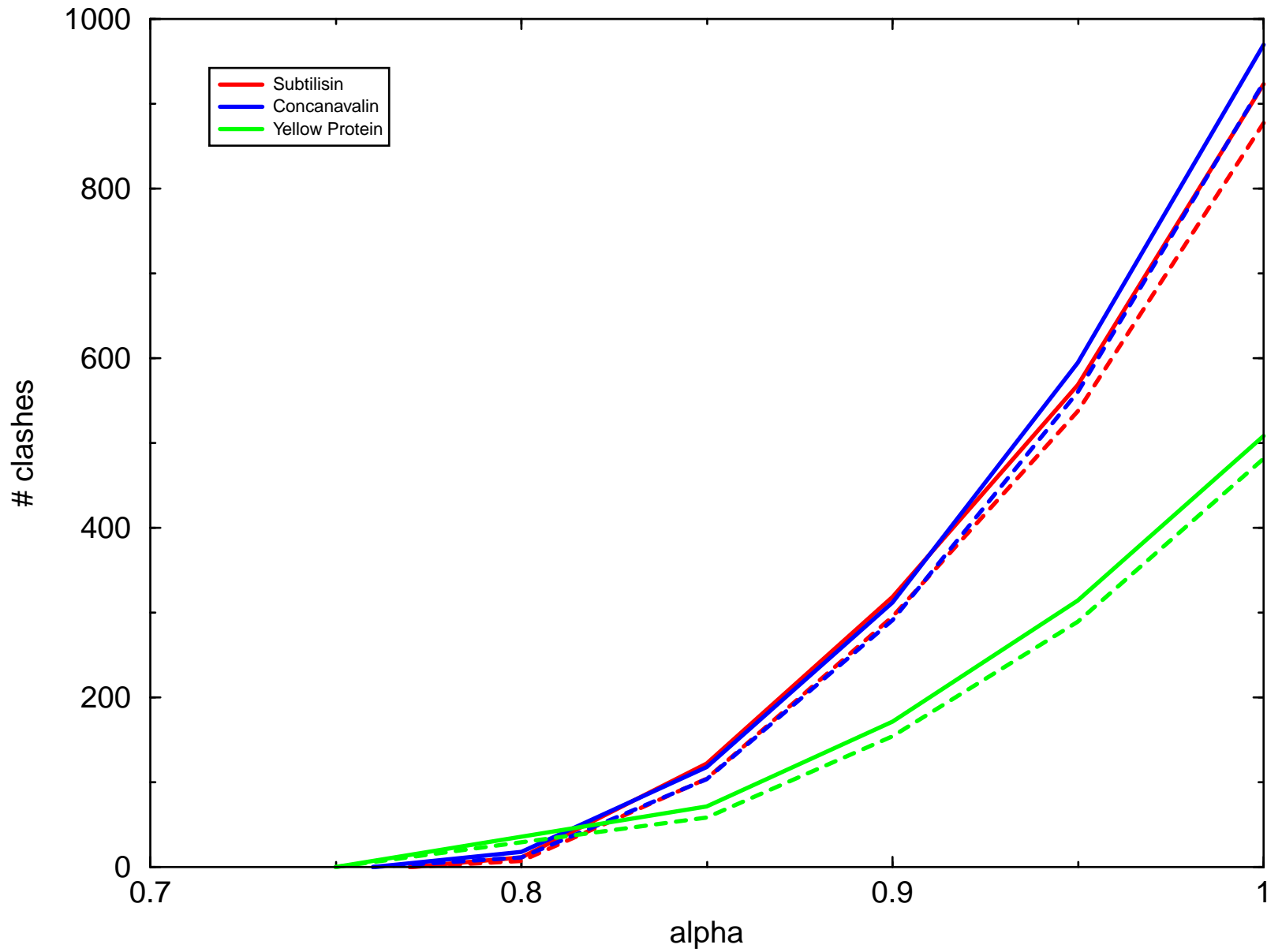
## Tables

protein	# of $\chi$ 's	# of res.	States per $\chi$ /per res.	S per $\chi$ /per res.
1F9I	99	49 (125)	1.52 / 2.33	0.42 / 0.85
1NLS	151	88 (237)	1.46 / 1.92	0.38 / 0.65
1GCI	174	100 (269)	1.39 / 1.78	0.33 / 0.58

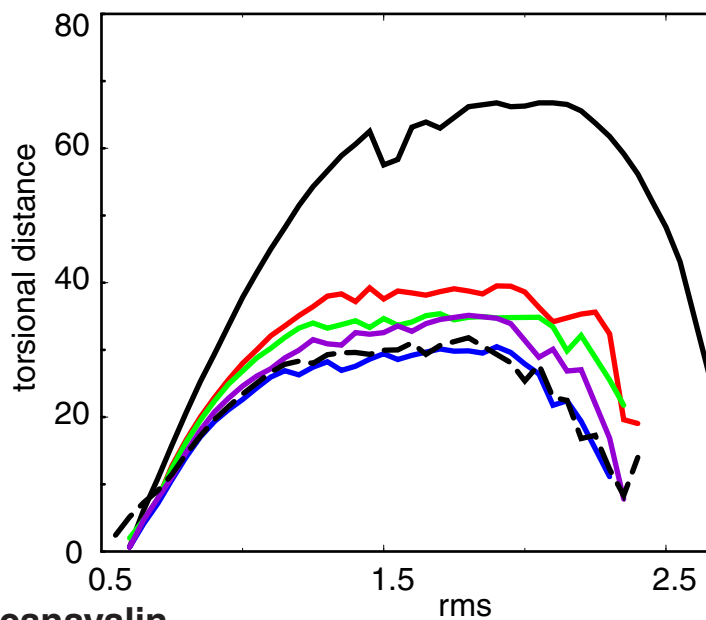
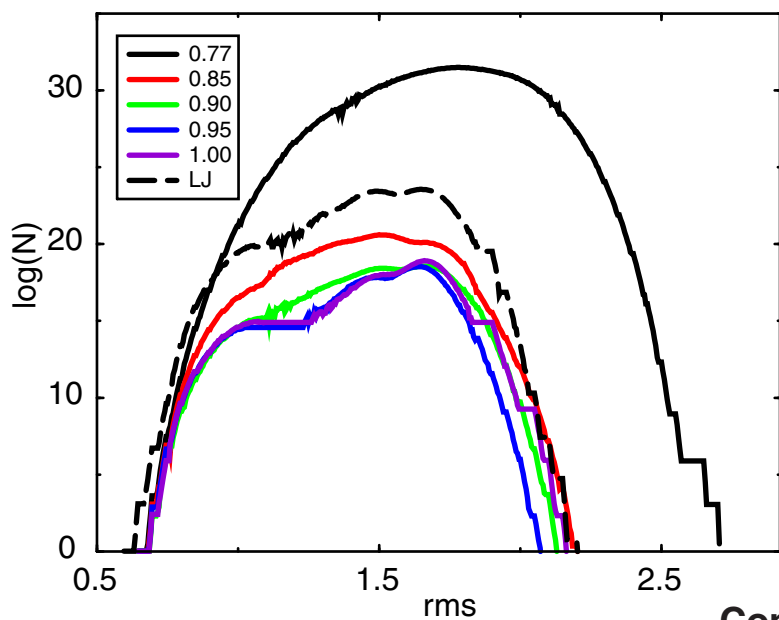
Table 2:

### Table 2

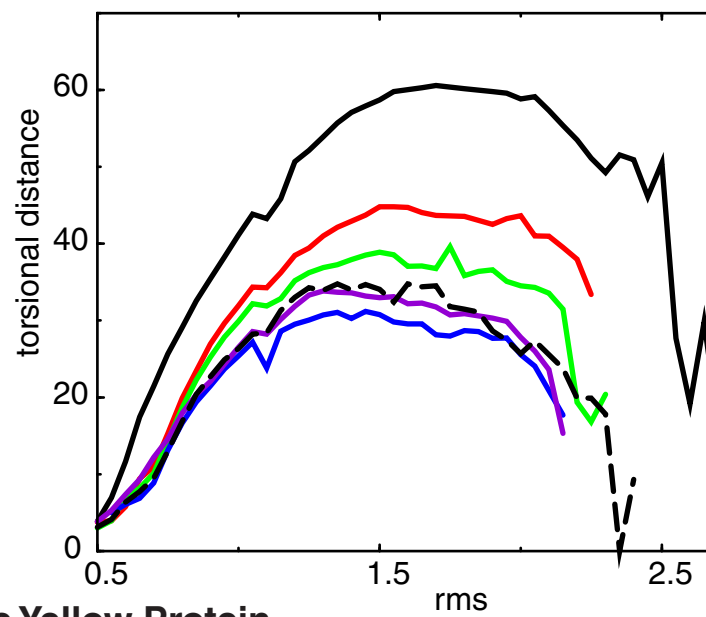
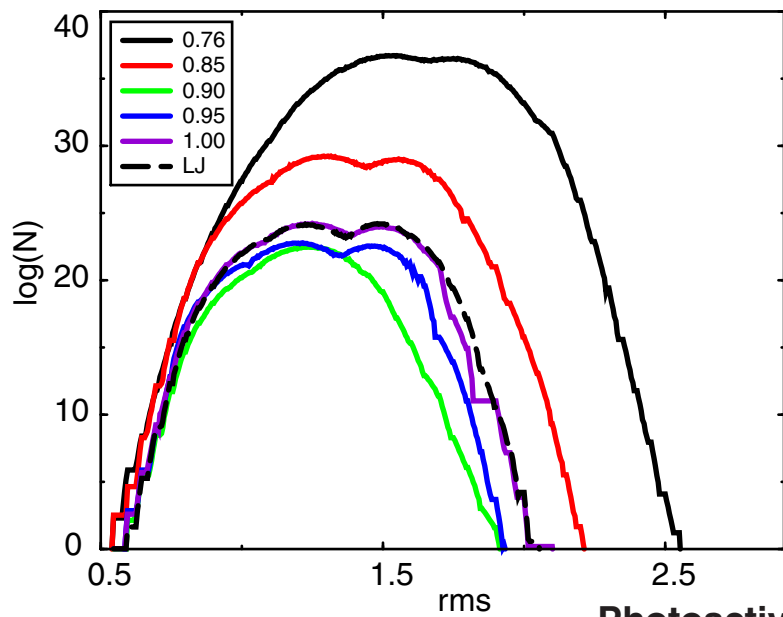
Statistics of repackings for photoactive yellow protein (1F9I), concanavalin (1NLS), and subtilisin (1GCI) using the repulsive Lennard-Jones model. The second column lists the number of torsions that contribute to the overall entropy. These torsions belong to residues having more than 40% occluded surface area. The number of occluded residues having one or more free torsions is given in the third column, with the total length of the protein in parentheses. The number of states and entropy (S) per  $\chi$  and per residue are calculated over the occluded residues only.



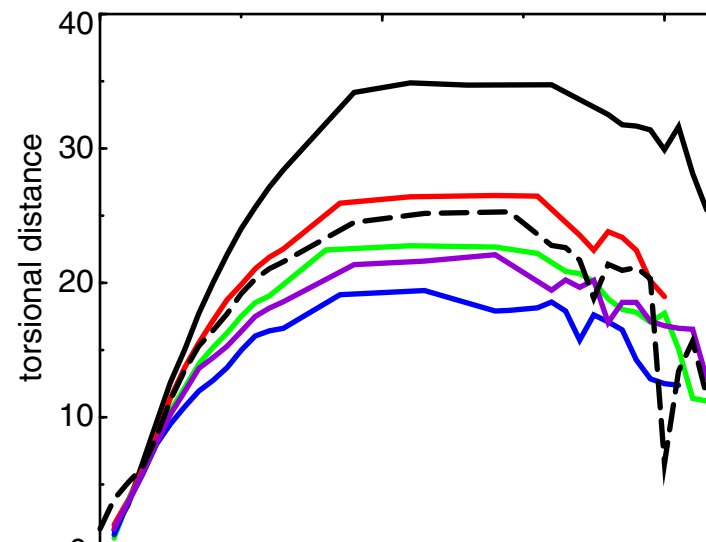
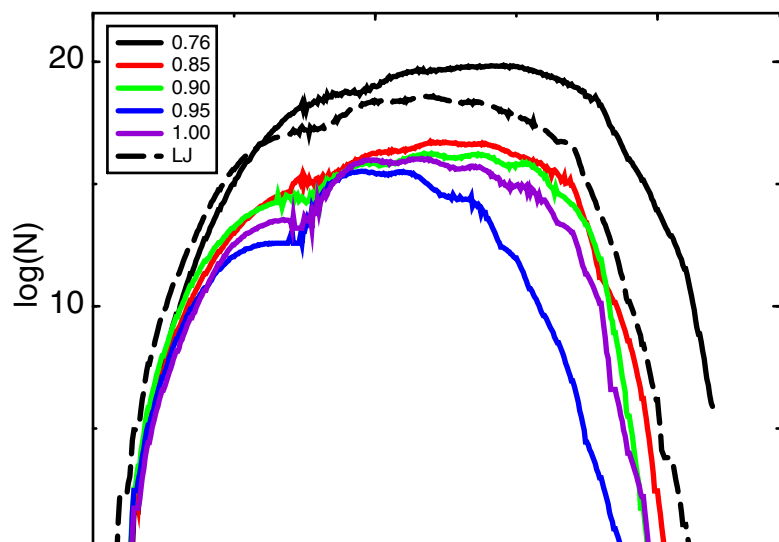
### Subtilisin

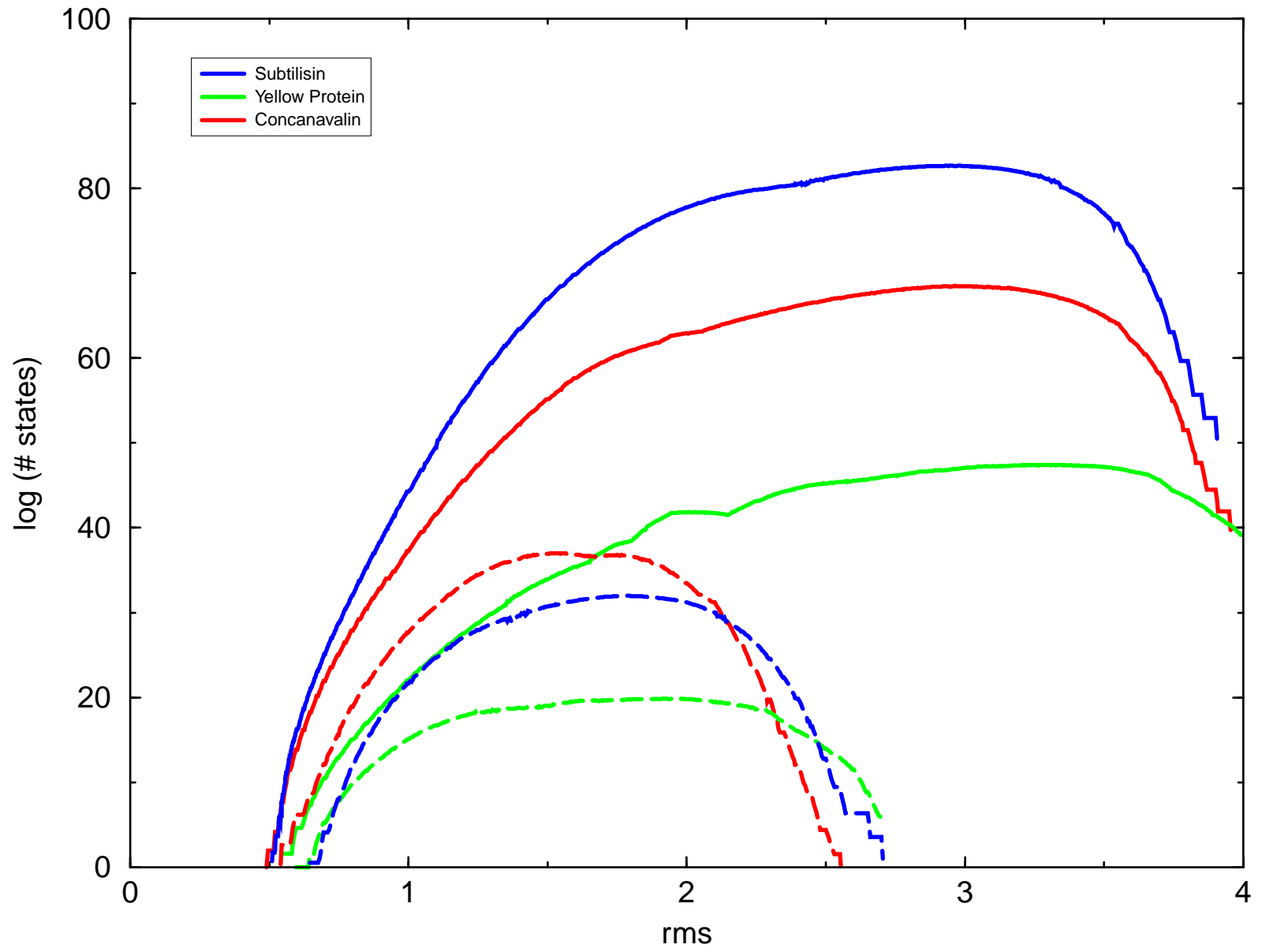


### Concanavalin

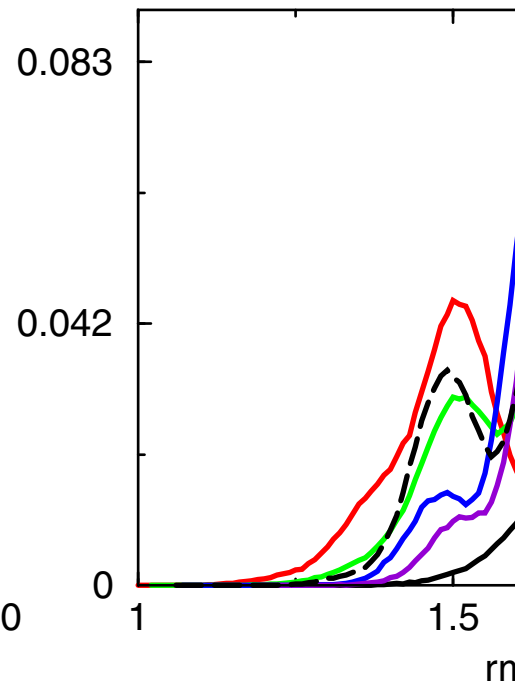
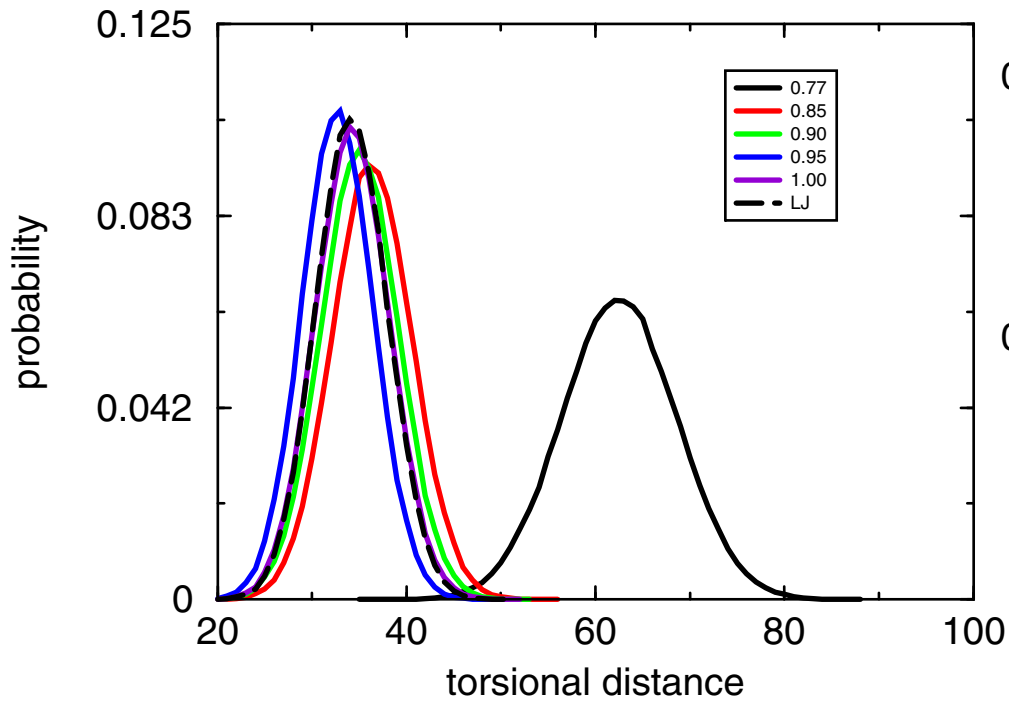


### Photoactive Yellow Protein









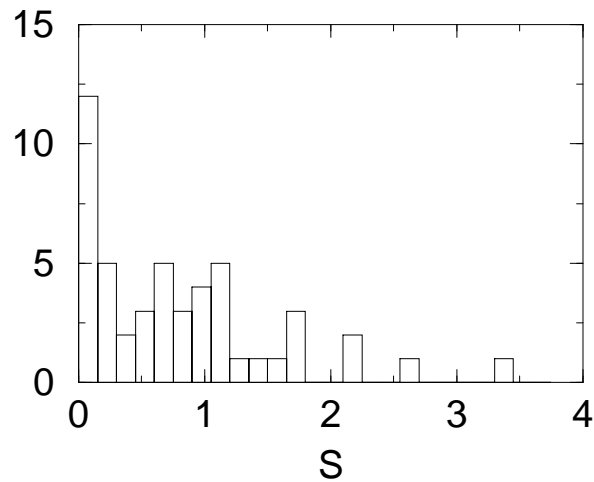
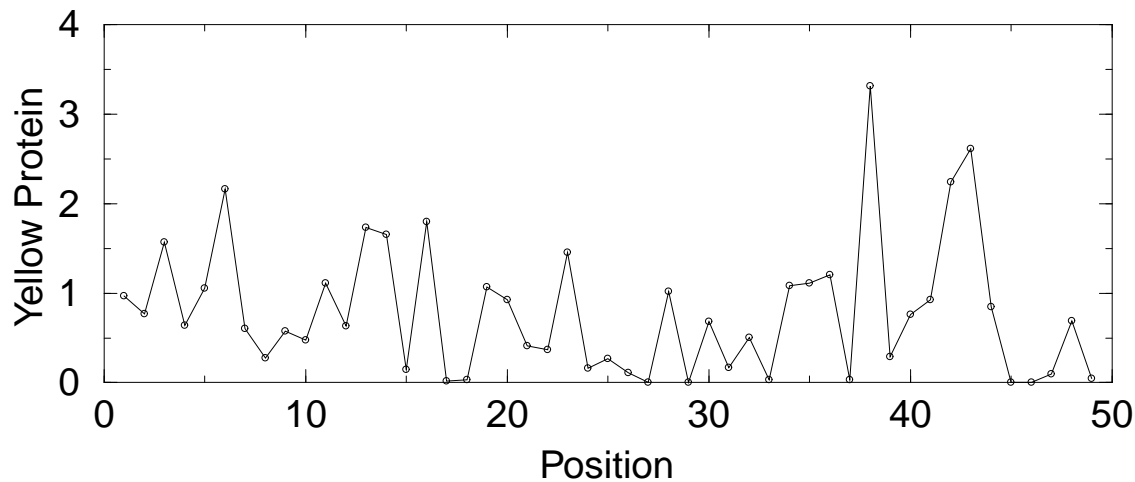
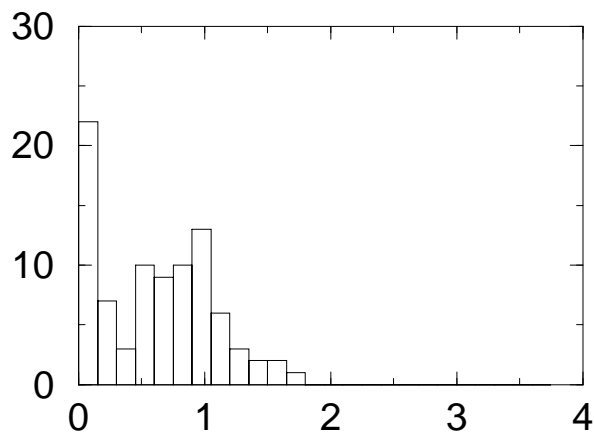
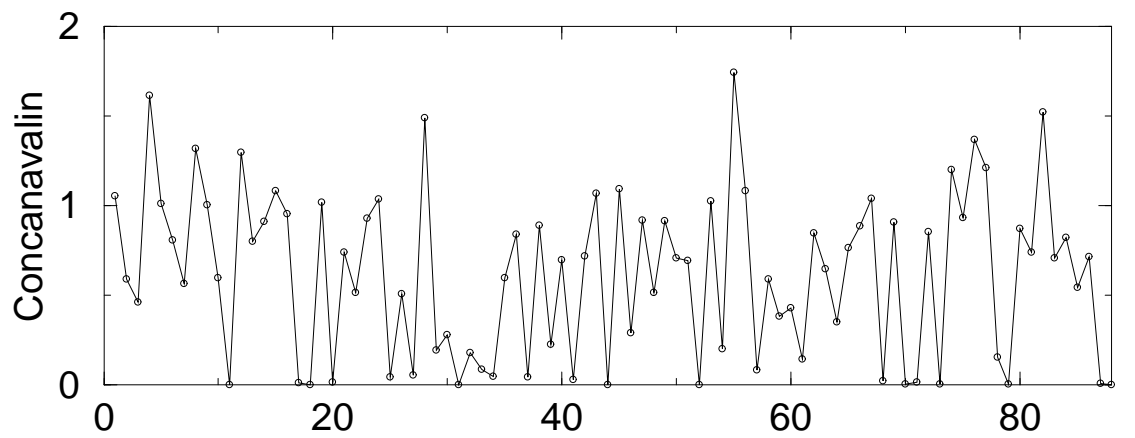
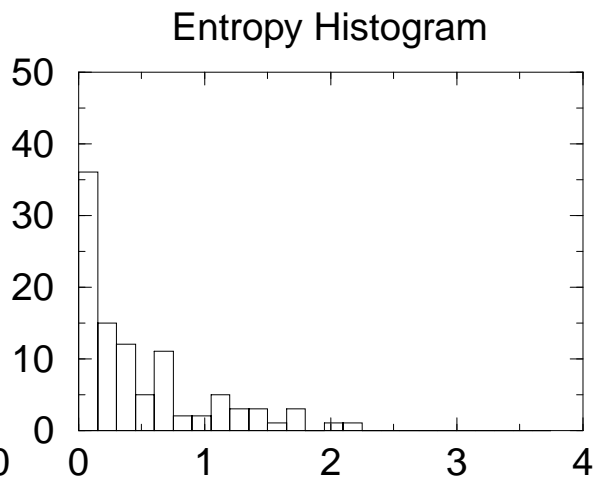
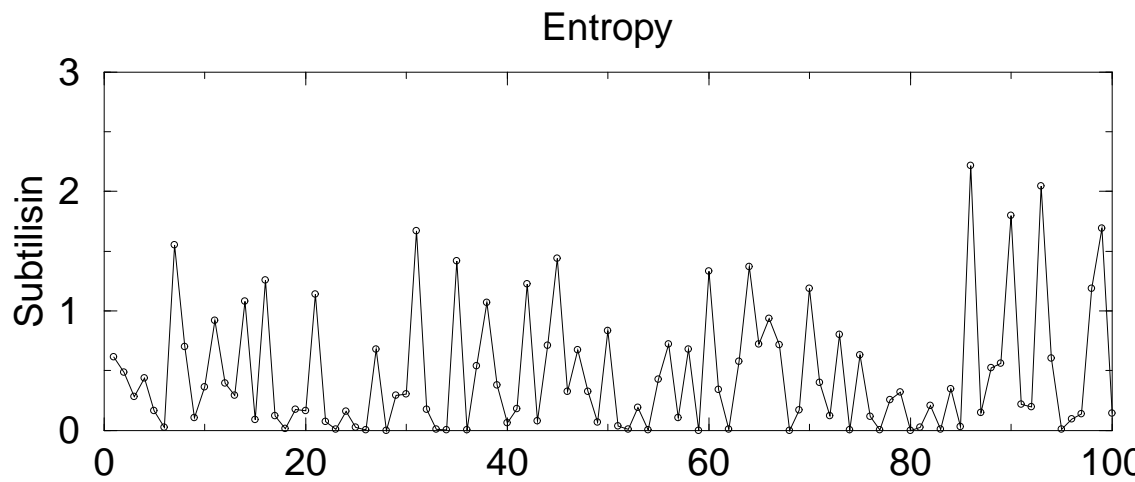




Figure 1:

Figure 2:

Figure 3:

Figure 4:

Figure 5:

Figure 6:

Figure 7: